Engineering Notes

Optimal Continuous/Impulsive Control for Lorentz-Augmented Spacecraft Formations

Ludwik A. Sobiesiak* and Christopher J. Damaren†
University of Toronto Institute for Aerospace Studies, Toronto, Ontario M3H 5T6, Canada

DOI: 10.2514/1.G000334

Nomenclature

a	=	semimajor axis
$\boldsymbol{b}$	=	magnetic field vector
e	=	eccentricity
$\boldsymbol{e}$	=	orbital element vector
$e^{(\cdot)}$	=	matrix exponential
f	=	true anomaly
h	=	angular momentum magnitude
i	=	inclination
J	=	cost
J_n	=	nth zonal harmonic coefficient
M	=	mean anomaly
m	=	mass
$\boldsymbol{m}$	=	magnetic dipole vector
$N-1$	=	number of thrusts
n	=	mean motion
p	=	semilatus rectum
q	=	electrical charge
r	=	orbit radius magnitude
$\boldsymbol{r}$	=	position vector
t	=	time
$\boldsymbol{u}$	=	continuous input/control vector
$\boldsymbol{v}$	=	velocity vector
$\boldsymbol{W}$	=	controllability Gramian
ΔV	=	delta-v magnitude
$\delta(t)$	=	Dirac delta function
$\boldsymbol{\zeta}$	=	differential element error
$\boldsymbol{\lambda}$	=	continuous co-state vector
μ	=	gravitational parameter
$\boldsymbol{\nu}$	=	discrete co-state vector
$\boldsymbol{\omega}$	=	angular velocity vector
$\boldsymbol{\Phi}$	=	state transition matrix
Ω	=	right ascension of ascending node
$\mathcal{H}_{c/d}$	=	continuous/discrete Hamiltonian
$(\cdot)^\times$	=	skew symmetric matrix operator

Subscripts

c	=	chief
d	=	deputy
L	=	Lorentz force-related
r	=	reference quantity
$\oplus$	=	Earth-related quantity

Superscripts

$\bar{(\cdot)}$	=	mean quantity
$(\cdot)^*$	=	optimal quantity
$(\cdot)^+$	=	postimpulse quantity
$(\cdot)^-$	=	preimpulse quantity
$\hat{(\cdot)}$	=	unit quantity

I. Introduction

THE use of the geomagnetic Lorentz force is considered in this paper for the purpose of spacecraft formation control. A spacecraft with an electrostatic charge will interact with the Earth's magnetic field and experience the Lorentz force. To employ the force as a means of actuation, the spacecraft must be able to store and modulate the charge in order to realize a desired acceleration.

Spacecraft in low Earth orbit (LEO) will accumulate a small amount of charge [1], due to the ambient plasma, but not in sufficient amounts to realize a significant Lorentz force. One possible way of spacecraft charging is through ion and electron beam emission. NASA's SCATHA mission [2] demonstrated that spacecraft surface potential can be controlled through charged particle emission. The storage of charge on a capacitive sphere surrounding the spacecraft has been proposed by Peck [3]. A large capacitive stocking was proposed by Streetman and Peck [4] as an alternative means of charge storage. In this work, it is assumed that a beam emission system is used for charge modulation and that the spacecraft has a means of charge storage; however, the feasibility of both control and storage of charge at the charge quantities required for spacecraft formation flight remains undemonstrated.

The use of the Lorentz force as a means of propellantless spacecraft actuation was first proposed by Peck [3]. Applications of the Lorentz force such as low-orbit ground track repetition, propellantless orbital maneuvers, insertion in Jovian orbit, and the augmentation of gravity-assist fly-bys have all been proposed [4–7]. Lorentz force actuation for spacecraft formation flight has been explored in [8–10].

In this paper, the control of a spacecraft formation in LEO using the Lorentz force actuation is considered. As will be shown within, an analysis of the controllability of this situation reveals that the relative spacecraft state is not fully controllable using only the Lorentz force. Previous papers that have considered formation flight have considered reduced problems, such as in-plane rendezvous and formation control. To render the full-state problem controllable, the combined use of impulsive thrusting with Lorentz force actuation is proposed. A novel continuous/discrete linear quadratic regulator (LQR) is formulated to combine the two modes of actuation in an optimal fashion. Previous work has considered the combination of continuous thrusting with the Lorentz force, as well as the nonoptimal combination of impulsive thrusting [11]. In this work, through judicious choice of weighting matrices, a significant reduction in thruster delta-V requirement compared with conventional impulsive formation-keep strategies is demonstrated with the hybrid LQR, Lorentz-augmented strategy.

Presented as Paper 2013-5240 at the AIAA Guidance, Navigation, and Control Conference, Boston, MA, 19–22 August 2013; received 17 October 2013; revision received 9 May 2014; accepted for publication 17 May 2014; published online 4 September 2014.

*Ph.D. Candidate, Spacecraft Dynamics and Control Laboratory, 4925 Dufferin Street.

†Professor, 4925 Dufferin Street. Associate Fellow AIAA.

II. Lorentz-Augmented Formation Flying Dynamics

Atmospheric drag and the J_2 zonal harmonic of the Earth's gravity field, resulting from the Earth's oblateness, are the two primary perturbations for spacecraft formations in LEO. We are interested in the case in which the spacecraft in formation have similar ballistic coefficients, and, consequently, the effect of drag is not significant compared with the effect of J_2.

The J_2 perturbation has three effects on a spacecraft's orbital elements: short-term oscillations, long-term oscillations, and secular drift. It is the last of these, the secular drift of elements, that results in formation degradation. To avoid expending additional control effort in correcting for short- and long-term oscillations, the set of mean orbital elements, in the sense of Brouwer [12], is adopted for describing the state of a spacecraft. The classic mean orbital element set of semimajor axis, eccentricity, inclination, right ascension of the ascending node, argument of periapsis, and mean anomaly, $\bar{\boldsymbol{e}} = [\,\bar{a} \quad \bar{e} \quad \bar{i} \quad \bar{\Omega} \quad \bar{\omega} \quad \bar{M}\,]^T$, evolves according to

$$\dot{\bar{\boldsymbol{e}}}(t) = \boldsymbol{A}(\bar{\boldsymbol{e}}) + \frac{\partial \boldsymbol{\epsilon}(\boldsymbol{e})^T}{\partial \boldsymbol{e}} \boldsymbol{B}(\boldsymbol{e})\boldsymbol{u}(t) \tag{1}$$

where $\boldsymbol{A}$ is the vector of the secular element drift rates

$$\boldsymbol{A}(\bar{\boldsymbol{e}}) = \begin{bmatrix} 0 \\ 0 \\ 0 \\ -\frac{3}{2} J_2 \bar{n} \left(\frac{R_\oplus}{\bar{p}}\right)^2 \cos \bar{i} \\ \frac{3}{4} J_2 \bar{n} \left(\frac{R_\oplus}{\bar{p}}\right)^2 (5\cos^2 \bar{i} - 1) \\ \bar{n} + \frac{3}{4} J_2 \bar{n} \sqrt{1-\bar{e}^2} \left(\frac{R_\oplus}{\bar{p}}\right)^2 (3\cos^2 \bar{i} - 1) \end{bmatrix} \tag{2}$$

$\boldsymbol{B}(\boldsymbol{e})$ is the matrix containing Gauss's variational equations (GVE) relating accelerations in the spacecraft body frame to changes in orbital elements:

$$\boldsymbol{B}(\boldsymbol{e}) = \begin{bmatrix} \frac{2a^2 e \sin f}{h} & \frac{2a^2 p}{Rh} & 0 \\ \frac{p \sin f}{h} & \frac{(p+R)\cos f + Re}{h} & 0 \\ 0 & 0 & \frac{R \cos\theta}{h} \\ 0 & 0 & \frac{R \sin\theta}{h \sin i} \\ -\frac{p \cos f}{he} & \frac{(p+R)\sin f}{he} & -\frac{R \sin\theta}{h \tan i} \\ \frac{b(p\cos f - 2Re)}{ahe} & \frac{b(p+R)\sin f}{ahe} & 0 \end{bmatrix} \tag{3}$$

where h is the orbit's specific angular momentum, R is the orbit radius, b is the orbit's semiminor axis, f is the true anomaly, θ is the true latitude, and $\boldsymbol{\epsilon}(\boldsymbol{e})$ is a function that transforms osculating elements to mean elements and can be found in [13]. For the purposes of designing a controller, $\partial\boldsymbol{\epsilon}/\partial\boldsymbol{e}$ can be approximated as identity because off-diagonal terms are of the order of J_2 or smaller [13]. For the purpose of controller design, mean orbital elements are suitable for use with the GVE, and the osculating to mean transformation can be approximated by the identity matrix [13]. The control acceleration $\boldsymbol{u}(t)$ is expressed in the spacecraft's local-vertical, local-horizontal (LVLH) frame, where the vector $\hat{\boldsymbol{h}}_r$ is in the direction of the chief's orbital radius, $\hat{\boldsymbol{h}}_h$ is aligned with the chief's angular momentum vector, and the vector $\hat{\boldsymbol{h}}_\theta$ completes the right-hand rule.

Let the mean differential orbital element error be

$$\boldsymbol{\zeta}(t) = \bar{\boldsymbol{e}}_d(t) - \bar{\boldsymbol{e}}_r(t) = \delta\bar{\boldsymbol{e}}(t) - \delta\bar{\boldsymbol{e}}_r \tag{4}$$

where $\bar{\boldsymbol{e}}_d = \bar{\boldsymbol{e}}_c + \delta\bar{\boldsymbol{e}}$, and $(\cdot)_r$, $(\cdot)_d$, and $(\cdot)_c$ denote the reference, deputy spacecraft, and chief spacecraft orbital elements, respectively. The linearized error dynamics are

$$\dot{\boldsymbol{\zeta}}(t) = \tilde{\boldsymbol{A}}\boldsymbol{\zeta}(t) + \boldsymbol{B}(\bar{\boldsymbol{e}}_r)\boldsymbol{u}(t) \tag{5}$$

where

$$\tilde{\boldsymbol{A}} \equiv \left.\frac{\partial \boldsymbol{A}}{\partial \bar{\boldsymbol{e}}}\right|_{\bar{\boldsymbol{e}}=\bar{\boldsymbol{e}}_r} = \begin{bmatrix} & \boldsymbol{0}_{3\times3} & \\ \frac{\partial \dot{\bar{\Omega}}}{\partial \bar{a}} & \frac{\partial \dot{\bar{\Omega}}}{\partial \bar{e}} & \frac{\partial \dot{\bar{\Omega}}}{\partial \bar{i}} \\ \frac{\partial \dot{\bar{\omega}}}{\partial \bar{a}} & \frac{\partial \dot{\bar{\omega}}}{\partial \bar{e}} & \frac{\partial \dot{\bar{\omega}}}{\partial \bar{i}} \\ \frac{\partial \dot{\bar{M}}}{\partial \bar{a}} & \frac{\partial \dot{\bar{M}}}{\partial \bar{e}} & \frac{\partial \dot{\bar{M}}}{\partial \bar{i}} \end{bmatrix} = \begin{bmatrix} \boldsymbol{0}_{3\times3} \\ \\ \boldsymbol{0}_{3\times3} \end{bmatrix} \tag{6}$$

The linearized term $\frac{\partial \boldsymbol{B}(\bar{\boldsymbol{e}}_c)}{\partial \bar{\boldsymbol{e}}}\delta\boldsymbol{e}$ is considered negligible and is not included in Eq. (5) per Breger and How [14], where it is concluded that the term is small and can be neglected for formations in LEO with relative positions and velocities of up to 25 km and 40 m/s, respectively.

The Lorentz force per unit mass experienced by a charged spacecraft and expressed in the LVLH frame is

$$\boldsymbol{f}_L(t) = \frac{q(t)}{m} \boldsymbol{v}_{\text{rel}}(t)^\times \boldsymbol{b}_\oplus(t, \boldsymbol{e}) \tag{7}$$

where $\boldsymbol{v}_{\text{rel}}$ is the velocity of the spacecraft with respect to the Earth's magnetic field and $\boldsymbol{b}_\oplus(t, \boldsymbol{e})$ is the Earth's magnetic field vector at the location of the spacecraft. The quantity $q(t)/m$ is the ratio of electrostatic charge to mass of the spacecraft and will be referred to as the specific charge. The operator $(\cdot)^\times$ denotes the skew-symmetric matrix:

$$\boldsymbol{a}^\times = \begin{bmatrix} 0 & -a_3 & a_2 \\ a_3 & 0 & -a_1 \\ -a_2 & a_1 & 0 \end{bmatrix}$$

The velocity relative to the Earth's magnetic field is

$$\boldsymbol{v}_{\text{rel}}(t) \equiv \boldsymbol{v}(t) - \boldsymbol{\omega}_\oplus^\times \boldsymbol{r}(t) \tag{8}$$

where $\boldsymbol{v}(t)$ and $\boldsymbol{r}(t)$ are the spacecraft's inertial velocity and position, and $\boldsymbol{\omega}_\oplus$ is the Earth's angular velocity.

The controllability of the relative differential element time-varying system with the Lorentz force as the sole input is now investigated. The Lorentz-augmented linearized dynamics of the deputy spacecraft's differential orbital elements are

$$\dot{\boldsymbol{\zeta}}(t) = \tilde{\boldsymbol{A}}\boldsymbol{\zeta}(t) + \boldsymbol{B}(\bar{\boldsymbol{e}}_r)\boldsymbol{v}_{\text{rel}}^\times(t)\boldsymbol{b}_\oplus(t, \bar{\boldsymbol{e}}_r)\frac{q(t)}{m} \tag{9}$$

where the spacecraft's position and velocity vectors, and the Earth's magnetic field and angular velocity vectors, are all appropriately expressed in the LVLH frame. A new input matrix is defined,

$$\tilde{\boldsymbol{B}}(t, \bar{\boldsymbol{e}}_r) \equiv \boldsymbol{B}(\bar{\boldsymbol{e}}_r)\boldsymbol{v}_{\text{rel}}^\times(t)\boldsymbol{b}_\oplus(t, \bar{\boldsymbol{e}}_r) \tag{10}$$

and the sole control variable is the charge-to-mass ratio $u(t) = q(t)/m$, such that

$$\dot{\boldsymbol{\zeta}}(t) = \tilde{\boldsymbol{A}}\boldsymbol{\zeta}(t) + \tilde{\boldsymbol{B}}(t, \bar{\boldsymbol{e}}_r)u(t) \tag{11}$$

The controllability of a linear time-varying system can be determined by evaluating the controllability Gramian $\boldsymbol{W}(t, t_0)$ defined as

$$\boldsymbol{W}(t_1, t_0) = \int_{t_0}^{t_1} \boldsymbol{\Phi}(t_1, \tau)\boldsymbol{B}(\tau)\boldsymbol{B}^T(\tau)\boldsymbol{\Phi}^T(t_1, \tau)\,\mathrm{d}\tau \tag{12}$$

where $\boldsymbol{\Phi}(t, \tau) = e^{\tilde{\boldsymbol{A}}(t-\tau)}$ is the state transition matrix of the system and $\boldsymbol{B}(t)$ is the input matrix of a generic linear time-varying system. If $\boldsymbol{W}(t_1, t_0)$ is nonsingular, then the system is controllable [15].

The semimajor axis and inclination of a charged spacecraft's orbit govern the behavior of the Lorentz force that it will experience. The controllability Gramian has been calculated for $t_0 = 0, t_1 = T$, where T is the orbital period, for a range of semimajor axes, from LEO ($a =$ 6478 km) to medium Earth orbit ($a =$ 16378 km) and for inclinations ranging from $i = 0^\circ$ to $i = 90^\circ$. It was found that for the entire spectrum of orbits tested, there is consistently one near-zero eigenvalue in the controllability Gramian, indicating that the linearized differential element dynamics are not controllable using only the Lorentz force. Figure 1 plots absolute value of the minimum eigenvalue and compares it to the magnitude of the next smallest eigenvalue.

The lack of controllability stems from the cross-product expression in the Lorentz force. For this reason, the force is always perpendicular to the inertial velocity of the spacecraft relative to the magnetic field. These results motivate the investigation of formation control strategies that combine thruster actuation with Lorentz force actuation.

III. Optimal Hybrid Lorentz Force/Impulsive Thrust Control

To render the relative dynamics controllable, Lorentz force actuation is augmented with impulsive thruster firings. Impulsive formation-keeping is an attractive formation-keeping strategy because the "quiet time" between thruster applications is desirable for scientific missions and the small, constant accelerations required by continuous strategies are typically too small to be continuously realized [16].

The problem becomes one of designing an optimal control law for a system with both continuous (Lorentz force) and discrete (impulsive thrust) control inputs. Such a system is known as a hybrid control system. For the linear time-varying case, the dynamics of such a system can be written as

$$\dot{\boldsymbol{x}}(t) = \boldsymbol{A}(t)\boldsymbol{x}(t) + \boldsymbol{B}(t)\boldsymbol{u}(t), \qquad t \neq t_k \tag{13}$$

$$\boldsymbol{x}(t_k^+) = \boldsymbol{C}_k\boldsymbol{x}(t_k^-) + \boldsymbol{D}_k\boldsymbol{v}_k, \qquad t = t_k \tag{14}$$

where $\boldsymbol{x}(t)$ is the state, $\boldsymbol{u}(t)$ is the continuous control input, $\boldsymbol{v}_k$ is an impulsive control input, and $t_k, k = 1, \ldots, N-1$ indicates different times at which the discrete dynamics are applied. Impulsive application time t_k is assumed to be prescribed, and the superscripts $(\cdot)^-$ and $(\cdot)^+$ denote, respectively, the instants immediately before and after the discrete dynamics are applied. In the notation, we will abbreviate the state just prior to and just after an impulse to $\boldsymbol{x}^\pm = \boldsymbol{x}(t_k^\pm)$.

The discrete dynamics and control introduce discontinuities in the states. Bryson and Ho [17] present a variational method for solving optimal control problems with states experiencing discontinuities at interior points. More recently, Hu et al. [18] applied the impulsive maximum principle, originally developed by Blaquière [19], to the problem of linear quadratic control of switched continuous systems with impulsive control. In this paper, the work in [18] is extended to explicitly show how the solution to Riccati equation behaves at the application of the discrete dynamics.

We seek to minimize the hybrid performance index:

$$J(\boldsymbol{x}, \boldsymbol{u}, \boldsymbol{v}_k) = \tfrac{1}{2}\boldsymbol{x}^T(t_f)\boldsymbol{S}\boldsymbol{x}(t_f) + \frac{1}{2}\sum_{k=1}^{N-1}[\boldsymbol{x}_k^{-T}\boldsymbol{Q}_k\boldsymbol{x}_k^- + \boldsymbol{v}_k^T\boldsymbol{R}_k\boldsymbol{v}_k] + \frac{1}{2}\sum_{k=0}^{N-1}\int_{t_k^+}^{t_{k+1}^-}[\boldsymbol{x}^T(t)\boldsymbol{Q}(t)\boldsymbol{x}(t) + \boldsymbol{u}^T(t)\boldsymbol{R}(t)\boldsymbol{u}(t)]\,\mathrm{d}t \tag{15}$$

where $\boldsymbol{Q} = \boldsymbol{Q}^T \geq 0$, $\boldsymbol{Q}_k = \boldsymbol{Q}_k^T \geq 0$, $\boldsymbol{R} = \boldsymbol{R}^T > 0$, $\boldsymbol{R}_k = \boldsymbol{R}_k^T > 0$, $\boldsymbol{S} = \boldsymbol{S}^T \geq 0$, $t_0^+ = t_0$, and $t_N^- = t_f$. The continuous and discrete Hamiltonians, respectively, are defined as

$$\mathcal{H}_c[t, \boldsymbol{x}(t), \boldsymbol{u}(t), \boldsymbol{\lambda}(t)] = \frac{1}{2}\boldsymbol{x}^T(t)\boldsymbol{Q}(t)\boldsymbol{x}(t) + \frac{1}{2}\boldsymbol{u}^T(t)\boldsymbol{R}(t)\boldsymbol{u}(t) + \boldsymbol{\lambda}^T(t)[\boldsymbol{A}(t)\boldsymbol{x}(t) + \boldsymbol{B}(t)\boldsymbol{u}(t)] \tag{16}$$

$$\mathcal{H}_d(t_k, \boldsymbol{x}_k^-, \boldsymbol{v}_k, \boldsymbol{\nu}_k) = \frac{1}{2}\boldsymbol{x}_k^{-T}\boldsymbol{Q}_k\boldsymbol{x}_k^- + \frac{1}{2}\boldsymbol{v}_k^T\boldsymbol{R}_k\boldsymbol{v}_k + \boldsymbol{\nu}_k^T(\boldsymbol{C}_k\boldsymbol{x}_k^- + \boldsymbol{D}_k\boldsymbol{v}_k) \tag{17}$$

where the continuous and impulsive dynamics are adjoined to the cost function using the continuous and discrete co-states $\boldsymbol{\lambda}(t)$ and $\boldsymbol{\nu}_k$, respectively. The cost function becomes

$$J(\boldsymbol{x}, \boldsymbol{u}, \boldsymbol{v}_k) = \frac{1}{2}\boldsymbol{x}^T(t_f)\boldsymbol{S}\boldsymbol{x}(t_f) + \sum_{k=0}^{N-1}\int_{t_k^+}^{t_{k+1}^-}[\mathcal{H}_c(t) - \boldsymbol{\lambda}^T(t)\dot{\boldsymbol{x}}(t)]\,\mathrm{d}t + \sum_{k=1}^{N-1}[\mathcal{H}_d(t_k) - \boldsymbol{\nu}_k^T\boldsymbol{x}_k^+] \tag{18}$$

Taking the first variation of J and setting it to zero yields the following conditions:

$$\boldsymbol{\lambda}(t_f) = \boldsymbol{S}\boldsymbol{x}(t_f) \tag{19}$$

$$-\dot{\boldsymbol{\lambda}}(t) = \left(\frac{\partial\mathcal{H}_c(t)}{\partial\boldsymbol{x}(t)}\right)^T = \boldsymbol{Q}(t)\boldsymbol{x}(t) + \boldsymbol{A}^T(t)\boldsymbol{\lambda}(t), \qquad t \neq t_k \tag{20}$$

$$\boldsymbol{\lambda}(t_k^-) = \left(\frac{\partial\mathcal{H}_d(t_k)}{\partial\boldsymbol{x}(t_k)}\right)^T = \boldsymbol{Q}_k\boldsymbol{x}(t_k^-) + \boldsymbol{C}_k^T\boldsymbol{\nu}_k \tag{21}$$

$$\boldsymbol{\lambda}(t_k^+) = \boldsymbol{\nu}_k \tag{22}$$

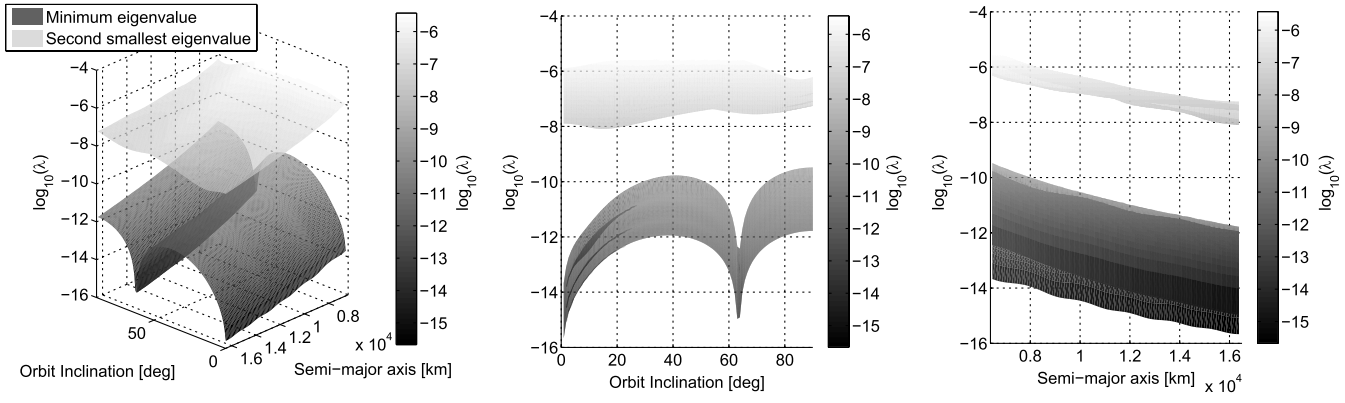

Fig. 1 Controllability plot of the differential orbital element system.

$$0 = \frac{\partial \mathcal{H}_c(t)}{\partial \boldsymbol{u}(t)}, \qquad t \neq t_k \tag{23}$$

$$0 = \frac{\partial \mathcal{H}_d(t_k)}{\partial \boldsymbol{v}_k} \tag{24}$$

Equations (23) and (24) yield the optimal control laws for continuous and discrete control inputs, respectively:

$$\boldsymbol{u}^*(t) = -\boldsymbol{R}^{-1}(t)\boldsymbol{B}^T(t)\boldsymbol{\lambda}(t) \tag{25}$$

$$\boldsymbol{v}_k^* = -\boldsymbol{R}_k^{-1}\boldsymbol{D}_k^T\boldsymbol{\lambda}(t_k^+) \tag{26}$$

Taking Eq. (13), with Eq. (25) substituted for $\boldsymbol{u}(t)$, together with Eq. (20) forms the continuous regulator two-point boundary value problem for the time interval $t \in [t_k^+, t_{k+1}^-]$, for which the linear relationship

$$\boldsymbol{\lambda}(t) = \boldsymbol{P}(t)\boldsymbol{x}(t) \tag{27}$$

with the terminal condition $\boldsymbol{P}(t_f) = \boldsymbol{S}$, is well known [15].

The optimal continuous feedback control is then

$$\boldsymbol{u}^*(t) = -\boldsymbol{R}^{-1}(t)\boldsymbol{B}^T(t)\boldsymbol{P}(t)\boldsymbol{x}(t), \qquad t \neq t_k \tag{28}$$

Substituting Eq. (27) and its temporal derivative into Eq. (20) yields the time-varying matrix Riccati equation:

$$-\dot{\boldsymbol{P}}(t) = \boldsymbol{A}^T(t)\boldsymbol{P}(t) + \boldsymbol{P}(t)\boldsymbol{A}(t) - \boldsymbol{B}(t)\boldsymbol{P}(t)\boldsymbol{R}^{-1}\boldsymbol{P}(t)\boldsymbol{B}^T(t) + \boldsymbol{Q}(t) \tag{29}$$

What remains is to determine how the solution to the Riccati equation changes after the application of an impulse. Immediately after the application of an impulse,

$$\boldsymbol{\lambda}(t_k^+) = \boldsymbol{P}(t_k^+)\boldsymbol{x}(t_k^+) \tag{30}$$

From Eqs. (21) and (22),

$$\boldsymbol{\lambda}(t_k^+) = \boldsymbol{C}_k^{-T}(\boldsymbol{P}(t_k) - \boldsymbol{Q}_k)\boldsymbol{x}(t_k^-) \tag{31}$$

The closed-loop impulsive dynamics become

$$\boldsymbol{x}(t_k^+) = [\boldsymbol{C}_k - \boldsymbol{D}_k\boldsymbol{R}_k^{-1}\boldsymbol{D}_k^T\boldsymbol{C}_k^{-T}(\boldsymbol{P}(t_k^-) - \boldsymbol{Q}_k)]\boldsymbol{x}(t_k^-) \tag{32}$$

where the optimal impulsive feedback control is

$$\boldsymbol{v}_k^* = -\boldsymbol{R}_k^{-1}\boldsymbol{D}_k^T\boldsymbol{C}_k^{-T}(\boldsymbol{P}(t_k^-) - \boldsymbol{Q}_k)\boldsymbol{x}(t_k^-), \qquad t = t_k \tag{33}$$

Equating Eqs. (30) and (31) and using Eq. (32), $\boldsymbol{P}(t_k^-)$ can be solved for as a function of $\boldsymbol{P}(t_k^+)$:

$$\boldsymbol{P}(t_k^-) = \boldsymbol{Q}_k + \boldsymbol{C}_k^T(\boldsymbol{1} + \boldsymbol{P}(t_k^+)\boldsymbol{D}_k\boldsymbol{R}_k^{-1}\boldsymbol{D}_k^T)^{-1}\boldsymbol{P}(t_k^+)\boldsymbol{C}_k \tag{34}$$

Applying the matrix inversion lemma and simplifying yields the discrete-time matrix Riccati equation:

$$\begin{aligned}\boldsymbol{P}(t_k^-) = {} & \boldsymbol{Q}_k + \boldsymbol{C}_k^T\boldsymbol{P}(t_k^+)\boldsymbol{C}_k \\ & - \boldsymbol{C}_k^T\boldsymbol{P}(t_k^+)\boldsymbol{D}_k(\boldsymbol{R}_k + \boldsymbol{D}_k^T\boldsymbol{P}(t_k^+)\boldsymbol{D}_k)^{-1}\boldsymbol{D}_k^T\boldsymbol{P}(t_k^+)\boldsymbol{C}_k\end{aligned} \tag{35}$$

What this means is that the solution to the continuous Riccati equation will experience discontinuities across impulse application times. To solve for $\boldsymbol{P}(t)$ for the optimal hybrid impulsive control problem, Eqs. (29) and (35) must be used in concert. The terminal error weight $\boldsymbol{P}(t_f)$ is set as the initial condition, and $\dot{\boldsymbol{P}}(t)$ is integrated backward using Eq. (29) from t_f to t_{N-1}^+. Integration is stopped at $t = t_{N-1}^+$, and $\boldsymbol{P}(t_{N-1}^-)$ is obtained from Eq. (35). $\boldsymbol{P}(t_{N-1}^-)$ is used as the new "initial" condition to resume integrating $\dot{\boldsymbol{P}}(t)$ until the next impulse time. Should the time-varying system be periodic, $\boldsymbol{P}(t)$ will also be periodic and the backward integration will yield a steady-state periodic solution.

IV. Numerical Examples

This section presents the results of numerical simulations that implement the proposed formation-keeping strategies. The numerical simulations integrate the inertial nonlinear equations of motion for both chief and deputy spacecraft:

$$\ddot{\boldsymbol{r}}(t) = -\frac{\mu}{r^3}\boldsymbol{r}(t) + \boldsymbol{f}_{J_2}(t,\boldsymbol{r}) + \boldsymbol{f}_L(t,\boldsymbol{r},\dot{\boldsymbol{r}}) + \sum_{k=1}^{N-1}\boldsymbol{v}_k\delta(t-t_k) \tag{36}$$

where μ is the Earth's gravitational constant. The Lorentz force $\boldsymbol{f}_L$ and the impulsive thrusts $\boldsymbol{v}_k$ are only applied to the deputy spacecraft; the chief is assumed to be uncontrolled. The only disturbance considered is the J_2 zonal harmonic. The IGRF-11 magnetic field model [20] is used to model the magnetic field. When solving the Riccati equations for the different LQR controllers, however, the simplified titled dipole model is used. Perfect state knowledge is assumed in all simulations.

For the hybrid impulsive/continuous LQR, the state penalty weights are chosen in a fashion that reflects the lack of controllability of the Lorentz-augmented relative spacecraft state. Consider the controllability Gramian $\boldsymbol{W}(t_1, t_0)$ given by Eq. (12). For a Lorentz-augmented system without impulsive control [Eq. (9) for all t], $\boldsymbol{W}(t_1, t_0)$ calculated for the desired orbit (where $t_0 = 0$ and $t_1 = T$) will typically have five nonzero eigenvalues and one zero eigenvalue. The eigenvectors of the nonzero eigenvalues, $\boldsymbol{\eta}_1 \ldots \boldsymbol{\eta}_5$, $\boldsymbol{\eta}_k \in \mathbb{R}^6$, represent the linear combinations of the states that are controllable by the Lorentz force. Likewise, the eigenvector corresponding to the zero eigenvalue $\boldsymbol{\eta}_0$ denotes the linear combination of states that is uncontrollable.

To minimize the thruster control effort being applied, it follows that the discrete portion of the hybrid LQR should only target the states that are uncontrollable by the Lorentz force. Conversely, the continuous portion of the LQR should target only the states that are controllable. To do so, the matrices $\boldsymbol{Q}$ and $\boldsymbol{Q}_k$ are obtained by

$$\boldsymbol{Q} = C_1[\,\boldsymbol{\eta}_1 \quad \boldsymbol{\eta}_2 \quad \boldsymbol{\eta}_3 \quad \boldsymbol{\eta}_4 \quad \boldsymbol{\eta}_5\,][\,\boldsymbol{\eta}_1 \quad \boldsymbol{\eta}_2 \quad \boldsymbol{\eta}_3 \quad \boldsymbol{\eta}_4 \quad \boldsymbol{\eta}_5\,]^T \tag{37}$$

$$\boldsymbol{Q}_k = C_2\boldsymbol{\eta}_0\boldsymbol{\eta}_0^T \tag{38}$$

where C_1 and C_2 are constants that scale the weights in an appropriate fashion. For the results that follow, $\boldsymbol{Q}$ and $\boldsymbol{Q}_k$ are kept constant. Having $\boldsymbol{Q}(t)$ and $\boldsymbol{Q}_k$ be time-varying remains unexplored at this time.

The spacecraft formation considered is a projected circular orbit. Chief mean orbital elements and deputy mean differential elements are given in Table 1.

Note that in order for all the relative states to be approximately the same order of magnitude, the differential semimajor axis state is normalized by the reference semimajor axis, $\delta\bar{a}/\bar{a}_r$. This results in equal LQR weighting for all the relative states. The terminal state penalty of $\boldsymbol{P}(t_f) = 10^{10} \cdot \boldsymbol{1}_{6\times6}$ is chosen. The control effort penalties are $R = 10^6$ and $\boldsymbol{R}_k = 10^8 \cdot \boldsymbol{1}_{3\times3}$ for continuous and impulsive controls, respectively. A single impulsive thrust per orbit is applied at a chief true anomaly of $f = 0$. The optimal impulse application time is not explored in this paper.

The Riccati solution that was obtained is periodic, but not with the period of the orbital motion; it has the same period as the magnetic

Table 1 Projected circular orbit initial conditions

	a, km	e, –	i, °	Ω, °	ω, °	M, °
$\bar{\boldsymbol{e}}_c$	7092	0.05	90.0	180.0	0.0	0.0
$\delta\bar{\boldsymbol{e}}$	0.0	0.0	8.0890×10^{-3}	0.0	-8.0789×10^{-2}	8.0688×10^{-2}

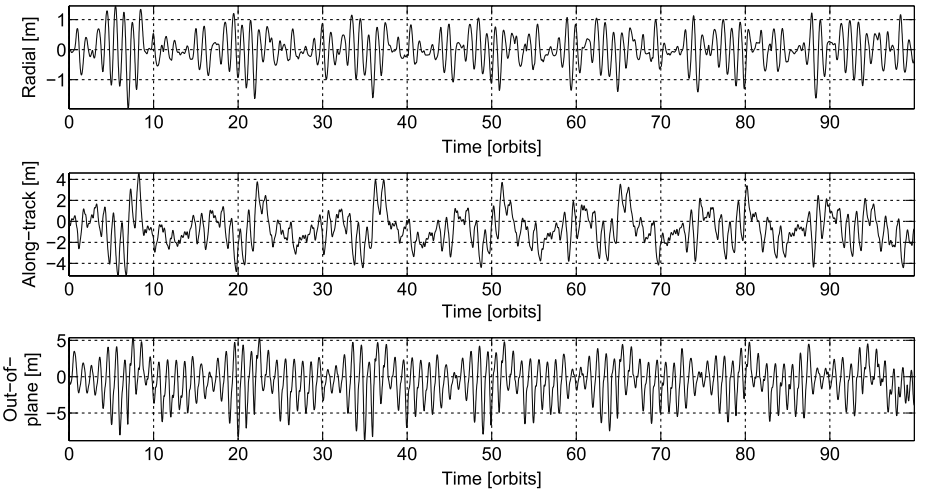

Fig. 2 Relative position error in the LVLH frame achieved with the Lorentz force and impulsive thrusting.

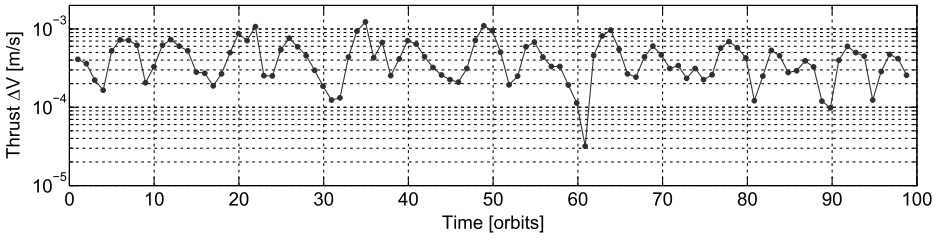

Fig. 3 Thrust magnitudes required for maintenance of a 1 km projected circular orbit using the hybrid LQR.

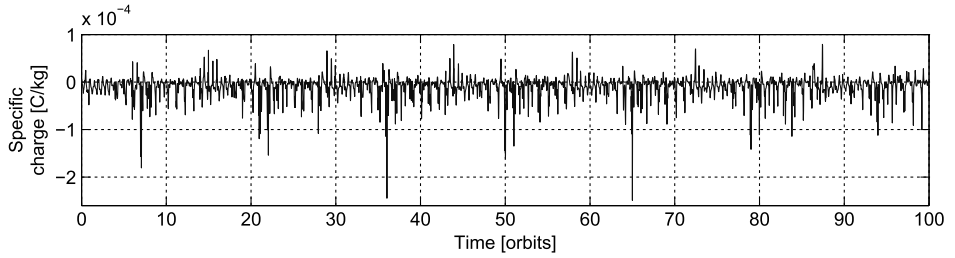

Fig. 4 Specific charges required for the maintenance of 1 km projected circular orbit using the hybrid LQR.

field. For a nontilted dipole model, this would be the same as the orbital period. For the tilted dipole model, however, the period of the magnetic field experienced by the spacecraft is basically one day.

The relative position error for a 100-orbit formation-keeping simulation using the hybrid LQR is shown in Fig. 2. The along-track and out-of-plane directions see the most error, with maximum errors of just over 4 and 5 m, respectively. The relative error in the radial direction is smaller, with a maximum of just over 1 m. The average total delta-V per orbit for this example was 17.73 mm/s, with thrusters providing an average of 0.4 mm/s per orbit and the remainder being provided by the Lorentz force. As can be seen in Fig. 3, individual thrust magnitudes are typically no larger than 1 mm/s. Thruster control effort is considerably smaller than that required by conventional thruster formation-keeping strategies. For comparison, the two-impulse scheme from [21] uses an average of 13.2 mm/s of delta-V per orbit to control the same formation considered here. The specific charge for this example is shown in Fig. 4 and has root-mean-square (RMS) and maximum absolute values of 2.11×10^{-5} and 2.49×10^{-4} C/kg, respectively. Per the assessment in [22], these specific charge magnitudes are within the range of what is considered achievable with existing technologies.

To employ the continuous/impulsive LQR, a numerical solution to the time-varying matrix Riccati equation is required, which can be calculated a priori to the launch of a mission, for a given set of reference orbital elements. Rather than storing the solution itself, the solution can be fitted with a Fourier series whose coefficients would require less memory than the entire time series of the Riccati solution. For the simulation results in the preceding section, a 500-term Fourier series approximates the solution to the Riccati equation for the continuous control; however, it was found that the best performance was achieved when the true values of the Riccati solution were used at the impulse application times $t = t_k^-$. It is recommended that the actual values obtained from Eq. (35) be stored and used for the impulsive control and not be approximated by the Fourier series.

V. Conclusions

A novel method for optimally combining continuous and discrete control inputs has been presented and applied to the Lorentz-augmented, formation-keeping problem. Employing the Lorentz force as a means of actuation was shown to considerably reduce thruster delta-V required for formation-keeping. However, perfect spacecraft state knowledge was assumed in the presented simulation, and the sensitivity of the control strategy to errors in knowledge of local magnetic field requires further investigation. Additionally, in the design of the hybrid LQR, constant state penalty matrices were employed, but investigating the use of time-varying matrices that reflect favorable dynamics performing corrections is worthwhile. Although the specific charge quantities required by the control strategy were within what is considered feasible with existing technology, there remains work to be done in designing the hardware necessary for a Lorentz-augmented spacecraft.

References

[1] Hastings, D., and Garrett, H. B., *Spacecraft-Environment Interactions*, Cambridge Univ. Press, Cambridge, England, U.K., 1996, p. 190.

[2] Garrett, H. B., "The Charging of Spacecraft Surfaces," *Reviews of Geophysics and Space Physics*, Vol. 19, No. 4, 1981, pp. 577–616. doi:10.1029/RG019i004p00577

[3] Peck, M., "Prospects and Challenges for Lorentz-Augmented Orbits," *AIAA Guidance, Navigation, and Control Conference and Exhibit*, AIAA Paper 2005-5995, 2005. doi:10.2514/6.2005-5995

[4] Streetman, B., and Peck, M., "General Bang-Bang Control Method for Lorentz Augmented Orbits," *Journal of Spacecraft and Rockets*, Vol. 47, No. 3, 2010, pp. 484–492. doi:10.2514/1.45704

[5] Streetman, B., and Peck, M., "New Synchronous Orbits Using the Geomagnetic Lorentz Force," *Journal of Guidance, Control and Dynamics*, Vol. 30, No. 6, 2007, pp. 1677–1689. doi:10.2514/1.29080

[6] Streetman, B., and Peck, M., "Gravity-Assist Maneuvers Augmented by the Lorentz Force," *Journal of Guidance, Control and Dynamics*, Vol. 32, No. 5, 2009, pp. 1639–1647. doi:10.2514/1.35676

[7] Atchison, J., and Peck, M., "Lorentz-Augmented Jovian Orbit Insertion," *Journal of Guidance, Control and Dynamics*, Vol. 32, No. 2, 2009, pp. 418–425. doi:10.2514/1.38406

[8] Peck, M. A., Streetman, B., Saaj, C., and Lappas, V., "Spacecraft Formation Flying Using Lorentz Forces," *Journal of British Interplanetary Society*, Vol. 60, July 2007, pp. 263–267.

[9] Pollock, G., Gangestad, J., and Longuski, J., "Analytical Solutions for the Relative Motion of Spacecraft Subject to Lorentz-Force Perturbations," *Acta Astronautica*, Vol. 68, No. 1, 2011, pp. 204–217. doi:10.1016/j.actaastro.2010.07.007

[10] Tsujii, S., Bando, M., and Yamakawa, H., "Spacecraft Formation Flying Dynamics and Control Using the Geomagnetic Lorentz Force," *Journal of Guidance, Control and Dynamics*, Vol. 36, No. 1, 2013, pp. 136–148. doi:10.2514/1.57060

[11] Sobiesiak, L., and Damaren, C., "Hybrid Periodic Differential Element Control Using the Geomagnetic Lorentz Force," *AIAA/AAS Astrodynamics Specialist Conference*, AIAA Paper 2012-4584, 2012. doi:10.2514/6.2012-4584

[12] Brouwer, D., "Solutions of the Problem of Artificial Satellite Theory," *The Astronomical Journal*, Vol. 64, No. 1274, 1959, pp. 378–396. doi:10.1086/107958

[13] Schaub, H., and Junkins, J. L., *Analytical Mechanics of Space Systems*, AIAA Education Series, AIAA, New York, 2003, pp. 533, 573–576.

[14] Breger, L., and How, J. P., "Gauss's Variational Equation-Based Dynamics and Control for Formation Flying Spacecraft," *Journal of Guidance, Control and Dynamics*, Vol. 30, No. 2, 2007, pp. 437–448. doi:10.2514/1.22649

[15] Kwakernaak, H., and Sivan, R., *Linear Optimal Control Systems*, Wiley-Interscience, New York, 1972, p. 64.

[16] Vadali, S. R., Yan, H., and Alfriend, K. T., "Formation Maintenance and Fuel Balancing for Satellites with Impulsive Control," *Astrodynamics Specialist Conference and Exhibit*, AIAA Paper 2008-7359, 2008. doi:10.2514/6.2008-7359

[17] Bryson, A., and Ho, Y., *Applied Optimal Control*, Hemisphere Publishing, New York, 1975, pp. 106–107.

[18] Hu, J., Wang, H., Liu, X., and Liu, B., "Optimization Problems for Switched Systems with Impulsive Control," *Journal of Control Theory and Applications*, Vol. 3, No. 1, 2005, pp. 93–100. doi:10.1007/s11768-005-0067-5

[19] Blaquière, A., "Necessary and Sufficient Conditions for Optimal Strategies in Impulsive Control and Applications," *New Trends in Dynamic System Theory and Economics*, edited by Aoki, M., and Marzollo, A., Academic Press, New York, 1979, pp. 183–213.

[20] Finlay, C. C., Maus, S., Beggan, C. D., Bondar, T. N., Chambodut, A., Chernova, T. A., Chulliat, A., Golovkov, V. P., Hamilton, B., Hamoudi, M., Holme, R., Hulot, G., Kuang, W., Langlais, B., Lesur, V., Lowes, F. J., Lühr, H., Macmillan, S., Mandea, M., McLean, S., Manoj, C., Menvielle, M., Michaelis, I., Olsen, N., Rauberg, J., Rother, M., Sabaka, T. J., Tangborn, A., Tøffner-Clausen, L., Thébault, E., Thomson, A. W. P., Wardinski, I., Wei, Z., and Zverevax, T. I., "International Geomagnetic Reference Field: The Eleventh Generation," *Geophysical Journal International*, Vol. 183, No. 3, 2010, pp. 1216–1230. doi:10.1111/j.1365-246X.2010.04804.x

[21] Sobiesiak, L., and Damaren, C., "Stability of an Impulsive Control Scheme for Spacecraft Formations in Eccentric Orbits," *Proceedings of the Institution of Mechanical Engineers, Part G: Journal of Aerospace Engineering*, Vol. 227, No. 10, 2013, pp. 1646–1659. doi:10.1177/0954410012462784

[22] Saaj, C., Lappas, V., Richie, D., Peck, M., Streetman, B., and Schaub, H., "Electrostatic Forces for Satellite Navigation and Reconfiguration," European Space Agency, Ariadna Final Rept. 05-4107b, 2006.